Acta Cryst. (1982). B**38**, 1877–1887

High-Pressure and High-Temperature Polymorphism of Iron Sulfide (FeS)

BY HUBERT E. KING JR* AND CHARLES T. PREWITT

Department of Earth and Space Sciences, State University of New York, Stony Brook, New York 11794, *USA*

(*Received* 11 *May* 1981; *accepted* 30 *October* 1981)

Abstract

The pressure- and temperature-induced phase transitions in FeS have been explored by X-ray diffraction measurements made on single-crystal samples. It is found that the room temperature and pressure structure, troilite (a close relative of the NiAs-type structure), with space group $P\bar{6}2c$ and a unit cell of $a = \sqrt{3}A$ and $c = 2C$ (where A and C refer to an NiAs-type structure and are approximately 3·4 and 5·9 Å, respectively), transforms at 420 K and ambient pressure, and at 298 K and 3·4 GPa to an MnP-type structure. This structure has space group *Pnma* and the orthohexagonal unit-cell dimensions $a = C$, $b = A$ and $c = \sqrt{3}A$. For FeS, the deviation of its unit cell from these ideal dimensions is small, and although the transformation results in a triply twinned crystal, the profiles of reflections containing contributions from multiple-twin domains are broadened but not split. A comparison of data from structure refinements adjacent to these transitions shows that, in both cases, the MnP-type phase has an increased distortion of the S atoms from planarity, a less distorted FeS_6 polyhedron, and longer Fe–Fe bonds. The differences in distortion between the structures suggests that their stabilities may depend upon the relative energy contributions from the distorted polyhedron and the Fe–Fe bond. Further increases in temperature produce a second-order transition to an NiAs-type structure, space group $P6_3/mmc$, whereas higher pressures cause an increasing sinusoidal distortion of the essentially h.c.p. S atoms. At 298 K and 6·7 GPa another transition takes place to an unknown structure. This transition is accompanied by a 9% volume change and a large decrease in C/A.

Introduction

At ambient conditions stoichiometric FeS is an antiferromagnetic semiconductor and has the troilite crystal structure. This structure is closely related to the NiAs-type structure and, as evidenced by the clustering of metal atoms into prism-like groups, apparently is stabilized through metal–metal bonding. This bonding seems to be strongly influenced by moderate changes in temperature and pressure, resulting in several phase transitions involving rearrangement of these clusters. The details of these transitions have been obscured in previous studies by several experimental difficulties that involve non-stoichiometric samples and unquenchable phases. This latter problem has especially hampered the structural characterization of the phases. We have, therefore, undertaken a structural study of FeS using iron-saturated single-crystal samples and *in situ* X-ray diffraction techniques. Our measurements were made as a function of temperature at ambient pressure and as a function of pressure at room temperature.

Previous work

High-temperature transitions

There are three phase transitions in FeS between room temperature and the breakdown temperature of approximately 1260 K. The lowest-temperature one occurs at approximately 420 K and is generally referred to as the α transition. It is a first-order transition, and previous workers have reported on the resulting changes in entropy (Robie & Waldbaum, 1968), electrical conductivity (Gosselin, Townsend & Tremblay, 1976), and magnetic susceptibility (Horwood, Townsend & Webster, 1976). The structural changes accompanying this transition have been investigated using diffraction techniques on powders with X-radiation (Haraldsen, 1941; Grønvold & Haraldsen, 1952; Taylor 1970), with neutrons (Andresen, 1960), and on single-crystal fragments with electron diffraction techniques (Putnis, 1974). All of these studies conclude that troilite transforms to an NiAs-type structure.

There are, however, several aspects of the data that are inconsistent with this conclusion. For example, Grønvold & Haraldsen pointed out that there were significant discrepancies between their observed intensities and those calculated assuming an NiAs-type structure. A similar type of disagreement was found for

* Present address: Exxon Research and Engineering Co., PO Box 45, Linden, New Jersey 07036, USA.

0567-7408/82/071877-11$01.00

the neutron diffraction data. In addition, the electron diffraction data contain superstructure spots that indicate a doubling of the *a* axis of the NiAs-type unit cell. Putnis, however, concludes that this phase, with a $2A-1C$ unit cell (*A* and *C* are used throughout this paper to denote the *a* and *c* axes of an NiAs-type unit cell), is metastable. As reported below, we have also found evidence for a similar phase and we believe our data show it to have a stability field.

At temperatures above that of the α transition, two additional transitions have been reported. At approximately 440 K there is a second-order, spin-flip transition (Sparks, Mead & Komoto, 1962; Andresen & Torbo, 1967; Horwood *et al.*, 1976), where the magnetic spins turn from being parallel to being normal to **c**. Although, there are no reports of any structural changes, there have not been detailed studies in this temperature range. The last transition is at the Néel temperature, approximately 600 K (Horwood *et al.*, 1976). No detailed structural investigations have been performed, but all available evidence indicates an NiAs-type structure above this temperature.

High-pressure transitions

At room temperature, there have been two transitions observed in investigations up to approximately 20 GPa. The lower-pressure one, 3·4 GPa, was found by Pichulo, Weaver & Takahashi (1976) who investigated the structural changes in FeS at high pressures using X-ray diffraction techniques on powders compressed within a diamond-anvil cell. Their data show that troilite transforms to a new phase whose powder pattern can be indexed with an NiAs-type unit cell except for three lines – at about 4·2, 1·8, and 1·25 Å (Pichulo, 1978).

The next transition is at 6·7 GPa (King, Virgo & Mao, 1978). The higher-pressure phase was shown by Pichulo *et al.* to be the same as that first discovered by Taylor & Mao (1970). The details of the structure of this phase are uncertain. Pichulo's (1978) model is a cell with orthorhombic symmetry; however, the presence of some lines which cannot be indexed suggests that this cell may be incorrect.

Experimental

Crystal synthesis

The crystals used in this study were synthesized from the elements in the form of iron foil and sulfur pieces. The iron was reduced under H_2 gas for 2 h at 1073 K immediately before its use. Then the elements were sealed in an evacuated silica-glass tube, reacted at 973 K for two weeks, and annealed at 373 K for four weeks. To insure metal-saturated samples, an excess of iron was always present. The numerous crystals produced were typically thin plates with polygonal outlines, ranging in size from 0·050 to 0·40 mm in diameter and from 0·020 to 0·10 mm thick. Their d_{102} values [2·093 (1) Å] are consistent with stoichiometric compositions (Yund & Hall, 1969). As reported below, we collected single-crystal X-ray intensity and unit-cell data on two of these crystals at room temperature and pressure. The unit-cell dimensions (Table 1) are in good agreement with those reported from stoichiometric powders: $a = 5{\cdot}9653$ (8), $c = 11{\cdot}750$ (2) Å (Yund & Hall, 1968); $a = 5{\cdot}966$ (1), $c = 11{\cdot}755$ (3) Å (Taylor, 1970). In addition, positional parameters obtained from least-squares refinement of the structure, for both data sets, match closely those from the most recent single-crystal study of troilite (Evans, 1970).

High-temperature measurements

High-temperature measurements were made using precession photography and four-circle diffractometry.

Table 1. *Unit-cell parameters for* FeS

T (K)	*P* (GPa)	Type*	*a* (Å)	*b* (Å)	*c* (Å)	α (°)	β (°)	γ (°)	*V* (Å³)	*C*/*A**
294	0·0001	$\sqrt{3}A-2C$	5·963 (1)	5·963 (1)	11·754 (1)	90·00 (1)	90·00 (1)	120·01 (1)	361·88 (9)	1·707
294	1·46 (5)	$\sqrt{3}A-2C$	5·922 (2)	5·924 (2)	11·689 (5)	90·04 (4)	89·98 (3)	119·99 (2)	355·2 (2)	1·709
294	2·99 (5)	$\sqrt{3}A-2C$	5·879 (4)	5·871 (4)	11·616 (4)	89·97 (5)	90·06 (5)	120·03 (4)	347·1 (3)	1·712
294	3·1 (1)	$\sqrt{3}A-2C$	5·875 (2)	5·876 (1)	11·618 (4)	90·03 (2)	89·95 (3)	119·99 (2)	347·4 (2)	1·712
294	3·08 (5)	$\sqrt{3}A-2C$	5·871 (4)	5·865 (4)	11·614 (3)	90·04 (5)	90·00 (4)	119·97 (4)	346·4 (3)	1·714
294	3·30 (5)	$\sqrt{3}A-2C$	5·870 (4)	5·865 (4)	11·607 (4)	89·99 (5)	90·05 (5)	120·01 (4)	346·0 (3)	1·713
294	3·33 (5)	$\sqrt{3}A-2C$	5·861 (3)	5·861 (2)	11·577 (7)	90·00 (5)	90·05 (4)	120·01 (3)	344·4 (3)	1·711
294	3·59 (5)	$2A-1C$	6·731 (5)	6·752 (4)	5·736 (6)	90·08 (6)	90·10 (7)	119·98 (3)	225·8 (3)	1·702
294	4·00 (5)	$2A-1C$	6·732 (5)	6·702 (10)	5·736 (6)	90·01 (8)	90·03 (5)	120·15 (5)	223·5 (3)	1·705
294	4·15 (5)	$2A-1C$	6·694 (9)	6·697 (7)	6·716 (9)	90·0 (1)	90·0 (1)	119·78 (7)	222·4 (5)	1·708
294	4·91 (5)	$2A-1C$	6·685 (4)	6·693 (3)	5·702 (8)	89·95 (6)	90·06 (8)	119·98 (3)	221·0 (3)	1·705
294	5·81 (5)	$2A-1C$	6·653 (6)	6·631 (6)	5·66 (1)	89·9 (1)	89·9 (1)	119·77 (6)	216·9 (5)	1·706
294	6·35 (5)	$2A-1C$	6·631 (8)	6·622 (7)	5·65 (1)	90·0 (1)	90·0 (1)	119·81 (6)	215·1 (5)	1·704
294	6·91 (5)	$2A-1C$	6·57 (3)	6·58 (2)	5·17 (6)	88·1 (6)	88·1 (6)	119·3 (2)	195 (2)	1·574
294	7·17 (5)	$2A-1C$	6·52 (2)	6·59 (2)	5·14 (4)	87·8 (4)	88·7 (5)	119·4 (2)	192 (2)	1·569
393 (20)	≪0·0001	$\sqrt{3}A-2C$	5·998 (11)	5·999 (8)	11·71 (1)	89·9 (1)	90·0 (1)	119·97 (9)	365·0 (8)	1·690
463 (20)	≪0·0001	$2A-1C$	6·935 (6)	6·930 (6)	5·825 (2)	90·02 (5)	89·96 (5)	120·00 (5)	242·4 (3)	1·680

* *A* and *C* represent the axial lengths for an NiAs-type cell. The structure is not necessarily that of the cell type; see text for details.

In both cases, Mo $K\alpha$ radiation was used, with a Zr filter for the precession camera and with a graphite monochromator for the diffractometer. The crystals were protected from oxidation by sealing them in evacuated glass capillaries. Heating was accomplished with a small resistance heater (Brown, Sueno & Prewitt, 1973). For these relatively low-temperature ($T < 500$ K) experiments, this heater has a large temperature uncertainty – approximately ± 20 K.

The unit-cell and integrated intensity data were collected on arbitrarily oriented crystals using the four-circle diffractometer. The unit-cell parameters were obtained by least-squares refinement of the centered angles for several large-2θ reflections using the technique of Tichý (1970). Integrated intensity data were collected by θ–2θ scans with the diffractometer in the bisecting setting. The intensity of a standard reflection was measured at fixed intervals throughout the data collection. A fixed-time count at the beginning and end of the scan was used to correct for background, and each reflection was corrected for Lorentz and polarization effects as well as crystal absorption. The absorption correction was computed using a modified version of Burnham's (1966) program with the absorption coefficients given by Hubbell, McMaster, Kerr Del Grande & Mallett (1974).

High-pressure measurements

With a few exceptions, the high-pressure diffraction measurements were made in a manner similar to that described above. Using the techniques of Finger & King (1978), each crystal was mounted in a Merrill & Bassett (1974)-type diamond-anvil cell. A 4:1 methanol–ethanol mixture was used as the hydrostatic pressure medium (Piermarini, Block & Barnett, 1973). Pressures were calibrated through wavelength measurements of the R_1 line from a small (<30 μm) chip of Cr-doped ruby that was placed within the sample chamber (Barnett, Block & Piermarini, 1973; Piermarini, Block, Barnett & Forman, 1975). The pressure uncertainty was 0·05 GPa (King & Prewitt, 1980). Crystals are partially blocked from view inside the diamond-anvil cell; thus, a diffracted-beam centering procedure (King & Finger, 1979) was used to align the crystals with the mechanical center of the diffractometer as well as to collect the data for least-squares refinement of the unit-cell parameters. The integrated intensity data were collected in the fixed-φ mode (Finger & King, 1978) using variable scan and background times. These were adjusted to give a fixed σ_I/I (Finger, Hadidiacos & Ohashi, 1973) within the restriction of a maximum time per reflection. Reflections whose θ's overlapped those for the four most intense beryllium diffraction rings were not measured. Interference resulting from diamond reflections is less systematic, and only three reflections were rejected because of such overlap. A correction for absorption by the diamond cell was made using a technique similar to that in Finger & King (1978). Corrections for Lorentz and polarization effects and crystal absorption were made as previously described.

Structure refinement

Least-squares refinements of all structures were accomplished using the program *RFINE*4 (Finger & Prince, 1975). This program minimized the function $\sum w(|F_o| - |F_c|)^2$, where the weight, w, for each reflection was set equal to $1/\sigma_F^2$. Only data with $I > 2\sigma_I$ were used in the refinements, and all data were averaged according to the space-group symmetry. All models used the scattering factors for neutral atoms from Cromer & Waber (1974).

Results and discussion

The troilite structure

A phase boundary extending from 420 K and 0·1 MPa to 298 K and 3·4 GPa defines the high temperature and pressure limits for the troilite structure. Within this pressure–temperature range, we collected data for three structure refinements as well as unit-cell-parameter data for determination of the compressibility.

The unit-cell-parameter data (Table 1) were collected at six pressures, including room pressure. Unconstrained cell refinements gave, within two standard deviations, hexagonal cell dimensions in all cases. The troilite unit cell is closely related to that of an NiAs-type. Their c axes are parallel and there is a 30° angle between their a axes (Fig. 2a). The relative axis lengths are $a = \sqrt{3}A$ and $c = 2C$. We determined the elastic constants, K_T and K_T' (the isothermal bulk modulus and its pressure derivative, respectively), by least-squares fitting of the unit-cell volumes to a third-order Birch–Murnaghan equation of state (Bass, Liebermann, Weidner & Finch, 1981). This gave $K_T =$ 82 (7) GPa and $K_T' = -5$ (4), where one standard deviation is enclosed in parentheses. Although K_T is typical for a moderately compressible material, the negative value for K_T' is unusual. For example, most materials have values between two and twelve. A negative K_T' indicates that the material becomes more compressible as its volume decreases, and such behavior has been found previously. Both cerium (Bridgman, 1927; Voronov, Vereshchagin & Goncharova, 1960) and AgI (Shaw, 1978) have polymorphs whose bulk moduli soften with increasing pressure as a phase transition is approached. For troilite a similar situation may exist; however, the negative value for K_T' must be considered tentative

because the volume measurements are poorly distributed across the range of pressures studied.

The fact that the same phase was found at both high temperature and high pressure was disconcerting until Navrotsky's (1980) paper discussing negative dT/dP slopes for lower-mantel transitions was published. For dT/dP to be negative, the Clausius–Clapeyron relation, $dT/dP = \Delta V/\Delta S$, requires ΔS to be positive if ΔV is negative. Electrical-conductivity measurements (King, 1979) show that troilite is a semiconductor and that the MnP-structure phase of FeS has metallic character, consistent with a positive change in entropy going from troilite to the MnP phase. Another observation, that the pressure derivative of the bulk modulus for troilite is negative, still needs further study; pyrrhotite has also been found to have a negative K'_T (Nakazawa, 1981, personal communication).

We refined the structural parameters using data collected at the following temperatures and pressures: 294 K and 0·1 MPa; 393 K and 0·1 MPa; and 294 K and 3·33 GPa. The room temperature and pressure data were collected from a small (0·05 × 0·05 × 0·11 mm) crystal that was mounted on a standard goniometer pin. Unlike the other data in this study, monochromatic Ag $K\alpha$ radiation was used for this data set. However, within two standard deviations, the refined parameters agree with those obtained using another crystal and Mo $K\alpha$ radiation. Of the 529 reflections collected, representing those with $h,k,l \geq 0$ and $0° < 2\theta < 50°$, 303 were symmetry-independent for space group $P\bar{6}2c$, and 271 of these had $I > 2\sigma_I$. We started our refinements from the positional parameters given by Evans (1970) and refined several models. The final model (Table 2*a*,*b*) included a scale factor, 6 positional parameters, and 14 anisotropic temperature factor coefficients. The unweighted residual was 0·039, and the weighted one, 0·034. Our positional parameters are in good agreement with those from Evans (1970); the largest difference is within three standard deviations. The temperature factor coefficients, however, differ significantly. This is probably because Evans did not apply an absorption correction to his data.

Data for the 393 K refinement were collected from a second small (0·08 × 0·08 × 0·10 mm) crystal. The 781 data, representing all reflections with $-5 \leq h, k \leq 5$; $0 \leq l \leq 6$; and $0° < 2\theta < 70°$, were reduced to 152 symmetry-independent reflections, of which 121 had $I > 2\sigma_I$. The refinement proceeded as above and the final model (Table 2*a*,*b*) was one containing anisotropic temperature factor corrections. This model gave 0·045 for the unweighted residual and 0·034 for the weighted one.

From a third crystal (0·04 × 0·10 × 0·15 mm) we collected data for the 3·33 GPa refinement. Except for reflections blocked by the diamond cell, we collected those with $0° < 2\theta < 70°$. These 1196 data contained three reflections that were rejected because of overlap with diamond reflections. Averaging led to 194 independent reflections of which 123 had $I > 2\sigma_I$. We refined several models, as above, and the final model was one containing isotropic temperature factor corrections. This model gave an unweighted residual of 0·068 and a weighted one of 0·053.

The troilite structure, first solved by Bertaut (1956), is related to the NiAs-type structure through small

Table 2. *Positional and thermal parameters for* FeS *in the troilite structure*

(*a*) Positional parameters (space group $P\bar{6}2c$)

T (K)		294	393 (20)	294	–*
P (GPa)		0·0001	≪0·0001	3·33 (5)	–
Fe[12(*i*)],	x	0·3787 (2)	0·3739 (2)	0·3779 (4)	$\frac{1}{3}$
	y	0·0553 (2)	0·0502 (2)	0·0556 (3)	0
	z	0·12300 (9)	0·1230 (3)	0·1228 (3)	$\frac{1}{8}$
S(1)[2(*a*)],	x	0	0	0	0
	y	0	0	0	0
	z	0	0	0	0
S(2)[4(*f*)],	x	$\frac{1}{3}$	$\frac{1}{3}$	$\frac{1}{3}$	$\frac{1}{3}$
	y	$\frac{2}{3}$	$\frac{2}{3}$	$\frac{2}{3}$	$\frac{2}{3}$
	z	0·0208 (2)	0·0186 (4)	0·0227 (8)	0
S(3)[6(*h*)],	x	0·6648 (6)	0·6658 (5)	0·665 (1)	$\frac{2}{3}$
	y	–0·0041 (4)	–0·0030 (6)	–0·0056 (7)	0
	z	$\frac{1}{4}$	$\frac{1}{4}$	$\frac{1}{4}$	$\frac{1}{4}$

(*b*) Temperature factor coefficients

T (K)		294	393 (20)	294
P (GPa)		0·0001	≪0·0001	3·33 (5)
	β_{11}†	0·0128 (4)	0·0171 (5)	–
	β_{22}	0·01111 (4)	0·0147 (5)	–
	β_{33}	0·00086 (4)	0·0036 (4)	–
	β_{12}	0·0064 (3)	0·0097 (4)	–
	β_{13}	–0·0001 (2)	–0·0001 (4)	–
	β_{23}	–0·0002 (2)	0·0003 (4)	–
	B (Å²)	0·988 (2)§	1·71 (8)§	1·09 (4)‡
S(1),	β_{11}	0·008 (1)	0·0098 (14)	–
	β_{22}	$=\beta_{11}$	$=\beta_{11}$	–
	β_{33}	0·0011 (2)	0·0014 (10)	–
	β_{12}	$=\beta_{11}/2$	$=\beta_{11}/2$	–
	β_{13}	0	0	–
	β_{23}	0	0	–
	B (Å²)	0·77 (6)§	0·96 (17)§	0·8 (1)
S(2),	β_{11}	0·0089 (7)	0·0089 (10)	–
	β_{22}	$=\beta_{11}$	$=\beta_{11}$	–
	β_{33}	0·0008 (2)	0·0032 (8)	–
	β_{12}	$=\beta_{11}/2$	$=\beta_{11}/2$	–
	β_{13}	0	0	–
	β_{23}	0	0	–
	B (Å²)	0·78 (4)§	1·2 (1)§	0·85 (9)
S(3),	β_{11}	0·0084 (9)	0·010 (1)	–
	β_{22}	0·0079 (10)	0·0088 (12)	–
	β_{33}	0·0011 (1)	0·0031 (8)	–
	β_{12}	0·0039 (8)	0·0047 (9)	–
	β_{13}	0	0	–
	β_{23}	0	0	–
	B (Å²)	0·79 (4)§	1·3 (1)§	0·68 (6)

* Positional parameters for an NiAs-type structure.
† The temperature factor expression is $\exp[-(\sum\sum h_i h_j \beta_{ij})]$.
‡ The temperature factor expression is $\exp(-B \sin^2\theta/\lambda^2)$.
§ Equivalent isotropic temperature factor (Hamilton, 1959).

displacements of the Fe and S atoms. The Fe atoms in an NiAs-type structure are six-coordinated by S atoms with each octahedron sharing edges with six octahedra in a plane normal to **c** and sharing faces with two others along **c**. In troilite, the Fe-atom displacements, which shorten two of the six Fe–Fe distances across those shared edges, link the Fe atoms into triangular groups (Fig. 2*a*) whose normals point along **c**. Across the shared face, these groups are paired into six-atom prisms. Such pairing is in contrast to the isolated triangular metal groups in NbS (Kadijk & Jellinek, 1969) and to the infinite linkages of similar groups in NiS, millerite (Rajamani & Prewitt, 1974). Across the intra-prism shared face, the Fe–Fe interaction seems to be repulsive; the metal–metal distance along the prism is longer than that between prisms. [Note: the distances in Evans (1970), Table 2, are reversed.] This repulsion along **c** is also seen in the unit cell's C/A ratio (Table 1, recalculated for an NiAs-type unit cell) which, of the structures studied, is largest for troilite. At ambient conditions the Fe-atom displacement is 0·305 Å.

Of the three symmetrically distinct S atoms, S(2) and S(3) are displaced from their ideal positions (Table 2*a*).

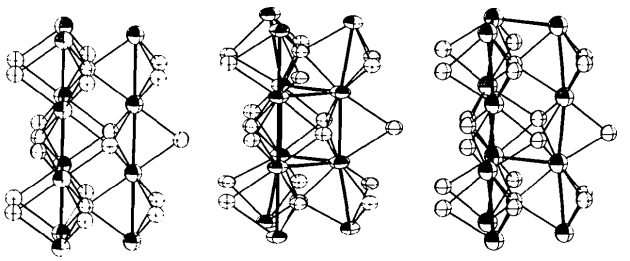

(*a*) (*b*) (*c*)

Fig. 1. A comparison of (*a*) the NiAs-type structure with (*b*) the troilite structure and (*c*) the MnP-type structure. In all three parts, the NiAs-type *c* axis points up and is slightly rotated out of the plane of the drawing. The metal atoms have sectioned ellipsoids.

The small displacement of S(3), 0·021 Å at ambient conditions, is constrained to be normal to **c**. Thus, two-thirds of the S atoms retain the planar S packing that is characteristic of the NiAs-type structure. The S(2) atoms, on the other hand, are displaced along **c** by 0·244 Å, and lie above and below the plane passing through the S(1) and S(3) atoms. This distortion is closely related to the formation of the Fe prisms. Each end of an Fe prism is capped by an S(2) atom (Fig. 1*b*), and that atom's displacement moves it away from the prism's end.

The displacement that draws the Fe atom into the triangular group also pulls it from the center of the surrounding S octahedron. The result is a very distorted coordination polyhedron. Of the six nearest neighbors, there is a 0·36 Å variation among the bond lengths (Table 3) making the coordination nearly fivefold. Not surprisingly, the longest bond is in the direction opposite to the Fe atom's displacement.

In common with many other structures, troilite becomes less distorted as the temperature increases. Between 294 and 394 K, displacements of the Fe and S(2) atoms decrease by 0·027 and 0·026 Å, respectively. Because of the Fe atom's decreased displacement as well as a decrease in C/A (Table 1), the prismatic Fe groups change shape significantly. The prism's height/width ratio goes from greater than one to less than one, mainly through large increases in the intra-triangular Fe–Fe distances coupled with essentially constant inter-triangular ones. Thus, face-sharing distances become shorter than edge-sharing ones, as they are in the NiAs-type structure. Accompanying this expansion of the Fe–Fe triangle, the S(2) atoms approach planar packing; z for S(2) decreases by about five standard deviations (Table 2*a*). Also, the Fe atom's coordination polyhedron becomes less distorted; for example, the quadratic elongation (Table 3) goes from 1·0195 to 1·0157.

Table 3. *Selected structural parameters calculated from the refined models of* FeS

T (K)	463 (20)	393 (20)	294	294	294	294
P (GPa)	≪0·0001	≪0·0001	0·0001	3·33 (5)	4·15 (5)	6·35 (5)
Structure	MnP	Troilite	Troilite	Troilite	MnP	MnP
Fe–S (Å)	2·461 (4)	2·370 (4)	2·360 (2)	2·323 (3)	2·396 (12)	2·349 (7)
	2·436 (4)	2·395 (5)	2·389 (2)	2·366 (7)	2·318 (18)	2·309 (7)
	2·461 (4)	2·436 (4)	2·422 (3)	2·393 (5)	2·396 (12)	2·349 (7)
	2·502 (4)	2·507 (4)	2·502 (2)	2·452 (5)	2·474 (10)	2·461 (6)
	2·502 (4)	2·554 (4)	2·560 (1)	2·513 (3)	2·474 (10)	2·461 (6)
	2·499 (5)	2·703 (5)	2·717 (2)	2·665 (4)	2·473 (13)	2·464 (6)
⟨Fe–S⟩ (Å)	2·477	2·494	2·492	2·452	2·422	2·399
FeS_6 QE*	1·0020	1·0157	1·0195	1·0202	1·0164	1·0198
Fe–Fe (Å)						
Edge-sharing	3·314 (4)	2·993 (5)	2·924 (2)	2·877 (3)	2·916 (11)	2·843 (5)
Face-sharing	2·918 (1)	2·927 (7)	2·947 (2)	2·899 (6)	2·904 (5)	2·878 (6)
Face-sharing	2·918 (1)	2·973 (7)	2·985 (2)	2·945 (6)	2·904 (5)	2·878 (6)

* Quadratic elongation (Robinson, Gibbs & Ribbe, 1971).

Unlike at high temperatures, only the S(2) atom's displacement changes significantly at high pressures. The Fe and S(2) atoms are displaced, respectively, 0·300 and 0·263 Å at 3·33 GPa. This shows that with increasing pressure the S atoms become increasingly non-planar. Despite a 5% decrease in cell volume and a significant C/A increase (Table 1), compression of the prismatic Fe group is isotropic. Its height/width ratio remains unchanged. The increase in quadratic elongation (0·0008) for the Fe atom's coordination polyhedron shows that there is only a small increase in its distortion.

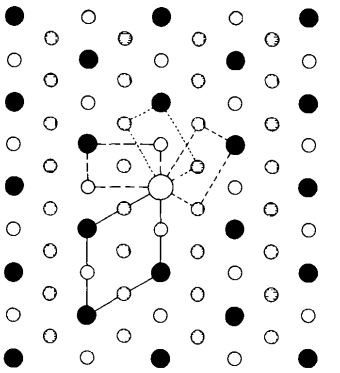

Fig. 2. Diffraction pattern for FeS with the MnP-type structure projected into the $hk0$ (NiAs-type) reciprocal net. NiAs-type diffraction spots are shown as filled circles, and the unit cell is outlined. The non-NiAs-type diffraction spots are divided into three sets, each set resulting from a single orthorhombic twin domain (dashed outlines). The figure is adapted from Wilson & Kasper (1964).

Structural changes at 420 K *and at* 3·4 GPa

We first examined the structural changes at these two transitions through precession photographs taken of FeS crystals at 448 K and 0·1 MPa and at 294 K and 3·59 GPa. At both high temperature and at high pressure, photographs from the $|00l|$ zone of an NiAs-type cell contained only NiAs-type reflections for the $hk0$ net; however, extra reflections accompanied these reflections on the $hk1$ and $hk2$ nets. The new diffraction patterns were, within experimental error, dimensionally hexagonal, and all diffraction spots could be indexed by doubling the a-axis repeat for an NiAs-type unit cell, giving a $2A$–$1C$ cell. Numerous tests – including measurements on additional crystals, tests for multiple diffraction effects, and cycling of the temperature and pressure through the transition to test for metastability – all indicated these diffraction effects to be intrinsic to FeS. [Although Putnis (1974) found a similar cell for FeS, his diffraction patterns contain cell-doubling reflections with $l = 0$. Thus, the two structures are apparently not equivalent.]

The $2A$–$1C$ indexing scheme accounts for all of the diffraction spots but indicates a systematic-absence rule that is not part of any hexagonal space group. The condition for the presence of an $hk0$ reflection is $h = 2n$ and $k = 2m$, where n and m are integers. Buerger (1936) has suggested that such non-space-group absences often indicate a twinned, lower-symmetry crystal, and the non-hexagonal intensity distribution we found for the cell-doubling reflections confirmed this was the case for FeS. Very similar diffraction patterns have been observed for MnAs at 328 K, and Wilson & Kasper (1964) showed that these diffraction effects are from three orthohombic twin domains that are related by 60° rotations around **c** of an NiAs-type cell (Fig. 2). According to this model, each substructure diffraction spot contains the contributions from three twin domains. We, therefore, scanned several large-2θ reflections for FeS in an attempt to resolve the individual reflections. Both ω and θ–2θ scans showed broadened profiles but no splitting. The diffuse nature of the reflections was also demonstrated in reduced precision of the unit-cell determinations and in apparent deviations from hexagonal symmetery (Table 1). However, even at the highest pressure, 6·35 GPa, no splitting was observed. Apparently, the orthorhombic unit cell for this FeS phase deviates only slighly from an orthohexagonal cell. If our reflections are indexed for this orthorhombic cell, the diffraction symbol is *mmmPn-a*, where **a** and **b** of the orthorhombic cell are coincident with, respectively, **c** and **a** of the NiAs-type one. We refined our structures, as did Wilson & Kasper, in the space group *Pnma* using the positional parameters for an MnP-type structure.

The MnP-*type structure*

To refine the elastic constants K_T and K_T' we collected unit-cell-parameter data at several intervals in the pressure range 3·6 to 6·4 GPa. Conversion from the $2A$–$1C$ unit cell to an orthorhombic one was made using the following: $a = c_{hex}$, $b = \langle a_{hex} \rangle/2$, and $c = \sqrt{3}b_{ortho}$. The elastic constants were determined as previously described except that in this case a stepwise refinement of V_0, the zero-pressure volume, was included because V/V_0 is required by the Birch–Murnaghan equation. The final parameters are $V_0 =$ 18·44 (4) cm^3 mol^{-1}, $K_T = 35$ (4) GPa, and $K_T' = 5$ (2). The difference in sign of K_T' between troilite and this phase makes ΔV for these phases a strong function of pressure with the room-temperature value for ΔV changing from plus to minus 0·28 cm^3 mol^{-1} in going from zero to 3·4 GPa. We believe this unusual pressure dependence, in part, explains a discrepancy between the calculated and observed dT/dP for the α transition (see the section *Phase relations*). The integrated-intensity data were collected as previously described, but wider detector slits were used to insure that the diffracted radiation from all of the twin domains was collected.

We prepared the data for use in the structure refinement using techniques similar to those described in Dollase (1965). First, the data were divided into four groups: overlapped reflections, those containing contributions from all three twin domains, and three groups of non-overlapped ones. Each of the latter groups represents an individual domain, and these data were used to determine the relative volumes for the domains. Structure refinement was then accomplished using both overlapped and one set of non-overlapped reflections (those from the largest-volume domain, V_1). The contributions, from the two lower-volume twin domains, to the intensities of the overlapped reflections are subtracted *via* the following:

$$I'_{hkl} = I^{\text{obs}}_{hkl} - s^2\left\{\frac{V_2}{V_1} I^{\text{calc}}_{h_2k_2l_2} + \frac{V_3}{V_1} I^{\text{calc}}_{h_3k_3l_3}\right\}. \qquad (1)$$

This correction was applied after each cycle of refinement, using that cycle's values for the scale factor (s), and the intensities of contributions from domains 2 and 3, $I^{\text{calc}}_{h_2k_2l_2}$ and $I^{\text{calc}}_{h_3k_3l_3}$.

Refinement of the MnP-type structure for FeS at high temperatures was accomplished using data collected at 463 K from the same crystal as that used at 393 K. We collected 822 reflections representing those with $-6 \le h, k \le 6$, $0 \le l \le 4$, and $0° < 2\theta < 70°$ for the $2A-1C$ cell. Of these, 606 had $I > 2\sigma_I$. Averaging and preparation as described above left a set of 190 data for use in the refinement. The structure was refined in space group *Pnma*, with both the Fe and S atoms occupying the 4(c) equipoint. Starting positional parameters were taken from FeAs (Selte & Kjekshus, 1973*a*). During the initial stages of the refinement we found that the scale factor was poorly constrained, with its variation from one cycle to the next being greater than three standard deviations, whereas the positional parameters changed by less than one. We believe that these large fluctuations result from the very unfavorable relative volumes for the twin domains, 1:0·99:0·60. Equation (1) shows that, for large values of V_2/V_1 and V_3/V_1, there is a strong correlation between the scale factor and the adjusted intensity, I'_{hkl}. To damp these fluctuations, we used a robust refinement technique (Prince & Nicholson, 1978) to refine further the parameters of the model. This allowed the refinement to converge and gave positional parameters within one standard deviation of those from the conventional refinement. Using the same technique, we refined the final model, which included isotropic temperature factors, and the parameters are listed in Table 4. For this refinement, 19 data had $|\Delta F/\sigma| > 15$ and were rejected leaving 171 reflections for which the residuals were 0·145, unweighted, and 0·104, weighted.

We collected integrated intensity data from crystals at two pressures. At 4·15 GPa, using the previously (3·33 GPa) described crystal, we collected those reflections with $0° < 2\theta < 65°$ that were not blocked by the diamond cell. Of these 661 data, 401 had $I > 2\sigma_I$ which yielded a data set of 68 reflections. Because refinement of a model that included variable temperature factors had large correlation coefficients between the scale factors and temperature factors, and, thus, would not converge, the final model (Table 4) was one having the temperature factors fixed at the values from the 3·33 GPa refinement. The unweighted residual was 0·149, and the weighted one was 0·159.

Table 4. *Refined parameters for* FeS *in the* MnP-*type structure* (*space group Pnma*)

T (K)		463	294	294	–‡
P (GPa)		<0·0001	4·15 (5)	6·35 (5)	–
Fe[4(c)],	x	0·0035 (3)	0·008 (2)	0·013 (1)	0
	y	¼	¼	¼	¼
	z	0·2352 (3)	0·206 (1)	0·2009 (4)	¼
	B (Å²)*	2·0 (1)	1·09†	0·67 (5)	–
S[4(c)],	x	0·2419 (5)	0·222 (2)	0·219 (1)	¼
	y	¼	¼	¼	¼
	z	0·5813 (8)	0·577 (2)	0·5792 (7)	7/12
	B (Å²)	1·2 (1)	0·76†	0·51 (7)	–

* The temperature factor expression is $\exp(-B \sin^2\theta/\lambda^2)$.
† Temperature factor held fixed during refinement – see text.
‡ Positional parameters for an NiAs-type structure.

The second high-pressure data set was collected at 6·35 GPa using another small crystal (0·03 × 0·09 × 0·11 mm). This crystal was mounted in the diamond-anvil cell as previously described, and within the restrictions imposed by the diamond-cell geometry, we collected those reflections with $l \ge 0$ and $0° < 2\theta < 70°$. Of these 368 reflections, 245 had $I > 2\sigma_I$ yielding a data set of 95 reflections. Refinement of the positional parameters, scale factor and isotropic temperature factors converged to give the parameters listed in Table 4, and the following residuals: 0·065, unweighted, and 0·080, weighted. These small residuals reflect the favorable domain-volume ratios, 1:0·33:0·31, for this crystal.

To compare our results with those from previous structural studies of FeS, we used the parameters of our models to calculate X-ray powder diffraction patterns. These calculations showed that at 4·15 GPa, and within the θ range recorded by Pichulo, six non-NiAs reflections should be observable in a powder pattern. Their d's, in order of decreasing intensity, are 1·831, 1·235, 1·810, 1·136, 1·357 and 4·071 Å. The extra diffraction lines reported by Pichulo can all be accounted for by these reflections but, possibly because of overlap of diffraction lines from the NaCl pressure medium, he did not observe the two at 1·357 and 1·136 Å. For 463 K, our calculations show that the intensities of these same reflections are an order of magnitude lower, which probably explains why past high-temperature diffraction studies have never ob-

served them. There have been, however, two other reflections recorded in such studies (Grønvold & Haraldsen, 1952; Taylor, 1970). Their d's are approximately 2·91 and 1·02 Å at 468 K (Taylor, 1977, personal communication), and according to Taylor (1970) the reflections are present for temperatures between T_α and T_N. The origin of these reflections is a mystery. They are not explained by our calculations nor through an appeal to possible contaminates, such as iron or iron oxide. One possible origin might be from a second iron sulfide phase. Mössbauer data (Gosselin, Townsend, Tremblay & Webster, 1976) indicate that $Fe_{0.996}S$, in this temperature range, consists of two phases in approximately 50:50 proportions. Materials with an MnP-type structure are typically stoichiometric (Selte & Kjekshus, 1973*b*); possibly, a narrow two-phase field exists between the MnP-type phase and a meta-deficient pyrrhotite.

The minor disturbance to the integrity of the single-crystal samples in going through the α transition implies a close relation between the MnP-type and troilite structures. Indeed, the structures adjacent to the transition have two features in common. In both, the Fe atom's main displacement is normal to the c axis of the NiAs-type cell, and the S atoms retain their essentially h.c.p. arrangement. According to Jellinek's (1959) classification scheme, distortion of the prototype structure, NiAs, should increase in going from troilite to MnP. However, the present data show that, for FeS, the trends in distortion are not clear. For example, the change from troilite to MnP-type decreases the FeS_6 polyhedral distortion but increases that of the S atoms from planarity. Although small, the differences in the two structures are significant and seem to be indicative of the stabilizing forces involved.

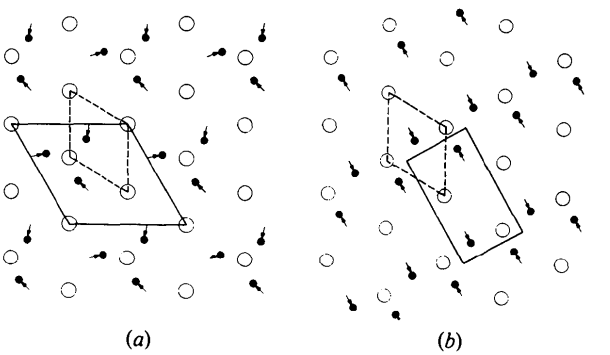

Fig. 3. The metal-atom displacements, shown with exaggerated magnitudes, in (*a*) the troilite structure and (*b*) the MnP-type structure, as viewed down **c** for an NiAs-type unit cell. The atom positions in an NiAs-type structure are indicated by the bases of the arrows.

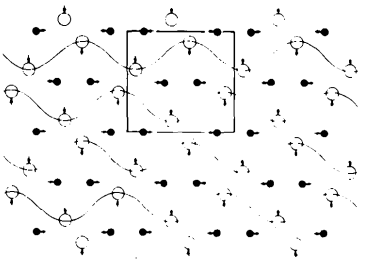

Fig. 4. The metal (filled circle) and non-metal atom displacements, both shown with exaggerated magnitudes, in the MnP-type structure (projected onto the *ac* plane of the unit cell; the displacements of the metal atoms are along **c**). The positions in an NiAs-type structure are shown by the bases of the arrows, and the sinusoidal distortion of the formerly planar non-metal atoms is indicated.

First, consider the Fe-atom displacements. These decrease in magnitude and change direction in transforming to the MnP-type structure. As a result, each Fe atom remains linked to two others across shared polyhedral edges, but now these linkages form continuous chains of atoms parallel to **b** (compare Fig. 3*a* and *b*). Also, the contacts across the shared polyhedral face change. Because of alternating metal-atom displacements along plus and minus **c** (Fig. 4), the stacking sequence for the Fe atoms changes from *AABBAA* ... (in troilite, Fig. 1*b*) to *ABAB* ... (Fig. 1*c*). As a consequence of these changes, the edge-sharing Fe–Fe bond lengths increase and the average face-sharing distances decrease at both T_α and P_α (Table 3). Thus, the MnP-type structure seems to have both reduced bond strength for the edge-sharing Fe–Fe contacts and increased shielding of the repulsion from adjacent face-sharing Fe atoms. The decrease in C/A (Table 1) gives further evidence for diminished repulsion across this face.

The S-atom displacements are also found to be distinctly different in the two structures. Although basically h.c.p., the plus and minus displacements along the normal to the h.c.p. planes (Fig. 4) impart a sinusoidal distortion, with $\lambda = |\mathbf{c}|$ and an amplitude proportional to the S atom's x coordinate. (In contrast, $\frac{2}{3}$ of the S atoms in troilite are coplanar.) This wave-like distortion and the Fe-atom movements are somehow interconnected as seen in Fig. 4, where succeeding waves along **a** form cavities with the Fe-atom chains at their centers. The origin of this, apparently repulsive, interaction is not clear, but the effect is strikingly similar to that found for the S(2) atom in troilite. Perhaps electrostatic repulsion is responsible. An excess charge build-up is associated with the formation of the triangular group (Bertaut, 1956; Goodenough, 1963, p. 282).

The interconnected Fe and S movements have a second important consequence, one that seems to give some insight into the stabilizing forces for troilite and the MnP-type structures. This is a variation in the FeS_6 polyhedral distortion, which, as shown by the decrease in quadratic elongation (Table 3), decreases at both T_α and P_α. In most instances, distortion of an octahedron

costs energy. Therefore, one factor that could stabilize the MnP-type structure is its lower, compared to troilite, octahedron-distortion energy. On the other hand, the discussion above showed that this structure also has a lower Fe–Fe bond strength. Possibly, the balance between these factors controls the relative stability of the two structures. It is clear that some force opposes that of the Fe–Fe bond since the distances in FeS (~2·9 Å) are longer than those predicted by metallic radii (2·5 Å). According to this model, the presence of the MnP-type structure for many different compounds, compared to the exclusive occurrence of the troilite structure for FeS, could indicate that the Fe–Fe bonds in FeS are particularly strong.

Although we did not collect data at higher temperatures for structure refinements, we monitored the intensities of the non-NiAs-type reflections, and found that between 360 and 490 K they dropped slowly below the detection limit and gradually increased again upon cooling. Apparently, the transition to the NiAs-type structure is second-order, as is that found for MnAs (Wilson & Kasper, 1964). Our relatively inaccurate temperature control prevented a more precise determination of the transition. However, this inaccuracy is not sufficient for the true transition temperature to be as high as T_N (600 K) where, as previously discussed, some unexplained diffraction peaks have been found.

With increasing pressure, the MnP-type cell compresses isotropically, and Table 1 shows that C/A is invariant up to 6·35 GPa. Despite this, the structure itself becomes more distorted. The Fe and S displacements at 6·35 GPa are 0·291 and 0·177 Å – a 12 and 8% increase, respectively, over those at 4·15 GPa. Over this pressure range, the edge-sharing Fe–Fe distance decreases considerably (0·073 Å or $\sim 9\sigma$), whereas the face-sharing one decreases by only 0·026 Å or $\sim 5\sigma$ (Table 3). Thus, the edge-sharing distance becomes shorter than the face-sharing one – a situation similar to that in the troilite structure. These changes in the intermetallic distances are accompanied by increased distortion of the octahedron (Table 3).

The 6·7 GPa *transition*

The diffraction patterns taken from a transformed single crystal differ from those of an MnP-type structure through the appearance of cell-doubling reflections on the $hk0$ net ($2A-1C$ indexing). However, precession photographs taken at the $l = \frac{1}{4}, \frac{1}{3}$, and $\frac{1}{2}$ levels between $hk0$ and $hk1$ did not reveal any additional reflections, and the patterns could be indexed with a $2A-1C$ unit cell. A second important change in going through the transition is that the slightly broadened reflection profiles became more diffuse and, in many instances, split. These broadened reflections made integrated intensity measurements impossible; therefore, only unit-cell data were collected using the diffractometer. In common with the MnP-type unit-cell data, incomplete separation of individual twin domains forced us to collect and refine the data for a hexagonal cell. The increased splitting and the difficulty in measuring such diffuse reflections are apparent in the size of the deviations from hexagonal dimensions and the estimated errors for the unit-cell parameters (Table 1). The volume change at the transition, calculated from these data and the compressibilities of the two phases, is $(-)1{\cdot}4\ \mathrm{cm^3\ mol^{-1}}$, approximately a 9% decrease.

This density change differs considerably from that calculated by Pichulo *et al.* (1976), 15%, and we believe this discrepancy is one indication that their model for the unit cell is incorrect. We also found, in comparing their powder patterns to our data, that one of their highest-intensity reflections is absent from our precession photographs. Assuming it to be 002 (for the $2A-1C$ cell), we can account for its absence and closely match its d, but their model indexes it as the 201 which, through transformation to the $2A-1C$ cell, should be visible on the $hk0$ precession photograph.

In our own, unsuccessful, search for an alternative unit cell we applied two standard indexing procedures – the Hesse–Lipson technique (Azároff, 1968, p. 490) and the 'zone search' method (de Wolfe, 1957; Visser, 1969). Even using the information on the precession photographs no single unit cell would satisfactorily fit a majority of the powder patterns. Our failure may indicate an inconsistency between the powder patterns and the precession photographs. It is possible that the NaCl pressure medium used in these powder diffraction studies has distorted the powder patterns either through non-hydrostatic stresses or through overlap of the diffraction lines.

If the unit-cell parameters in Table 1 are examined, it is found that the volume change results mostly from an abrupt decrease in the c-axis length. The C/A ratio decreases from approximately 1·70 to 1·57 across the transition. The deviation of this ratio from that for hexagonal closest-packing of the non-metal atoms (1·63) is generally attributed to metal–metal interactions across the shared face of the metal–sulfur octahedra. Consequently, the observed change in C/A may indicate increased metal–metal attraction along this direction.

Phase relations

The structure–temperature–pressure relationships inferred for FeS are summarized in Fig. 5, where data pertaining to the zero-pressure and high-pressure room-temperature transitions have already been discussed in the section *Previous work*. The pressure dependencies of these transitions, however, require further discussion.

The negative slope for the troilite-to-MnP phase boundary – as indicated by DTA (Kullerud, Bell &

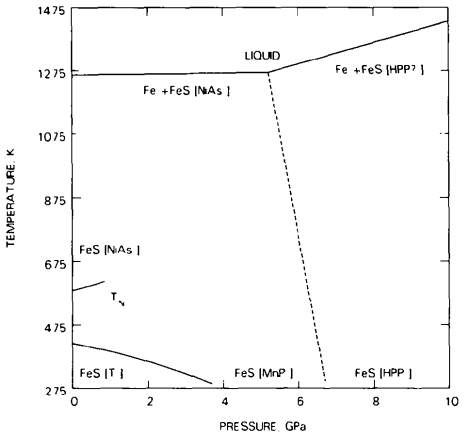

Fig. 5. The phase relations of FeS [structure types are indicated in square brackets (T = troilite and HPP = 'High-Pressure Phase')] as determined by data which are described in the text.

England, 1965) and electrical-resistance data (King, 1979) as well as the structural information from the present study – requires that the slope, which is approximately +23 K GPa^{-1} at zero pressure, change sign at elevated pressure. It can be shown (King, 1979) that a large, negative d^2T/dP^2 is a direct consequence of the compression behavior measured for these two phases in the present study; further, taking this derivative into account, qualitative agreement is obtained between the observed and calculated phase boundaries. The pressure dependencies of the second-order spin-flip and MnP-to-NiAs transitions are unknown, but Anzai & Ozawa (1974) have obtained a slope of +32(1) K GPa^{-1} for T_N in measurements taken up to 0·85 GPa. Through determinations of the eutectic melting temperature for Fe + FeS (Brett & Bell, 1969; Usselman, 1975), the incongruent melting point of FeS has been found to be nearly pressure independent up to 5·2 GPa, acquiring a linear pressure dependence of approximately 30 K GPa^{-1} above this pressure. This break, at about 5·2 GPa and 1270 K, has been proposed by Usselman to represent the intersection of the eutectic phase boundary with one for a low-to-high-density phase transition in FeS. Assuming this to be the case, this second phase boundary is probably an extension of the one at 6·7 GPa and room temperature, as shown in Fig. 5 by the dashed line. The available evidence, namely the absence of other high-pressure transitions in both static (Pichulo, 1978) and dynamic (King & Ahrens, 1973) high-pressure experiments and the ubiquitous high-density, non-quenchable nature of this phase reported by each study, suggests that the FeS ('High-Pressure Phase') occurs over this wide temperature–pressure range.

We thank Drs R. Liebermann and S. Weaver for their discussions regarding several aspects of this work. Our thanks also go to Mr K. Baldwin for his assistance with the experiments and to Mrs E. M. McCarthy for typing the manuscript. This work was supported by the National Science Foundation, grant EAR 77-13042.

References

ANDRESEN, A. F. (1960). *Acta Chem. Scand.* **14**, 919–926.
ANDRESEN, A. F. & TORBO, P. (1967). *Acta Chem. Scand.* **21**, 2841–2848.
ANZAI, S. & OZAWA, K. (1974). *Phys. Status Solidi*, **24**, K31–K34.
AZÁROFF, L. V. (1968). *Elements of X-ray Crystallography* New York: McGraw-Hill.
BARNETT, J. D., BLOCK, S. & PIERMARINI, G. J. (1973). *Rev. Sci. Instrum.* **44**, 1–9.
BASS, J. D., LIEBERMANN, R. C., WEIDNER, D. J. & FINCH, S. J. (1981). *Phys. Earth Planet. Inter.* **25**, 140–158.
BERTAUT, E. F. (1956). *Bull. Soc. Fr. Minéral. Cristallogr.* **79**, 276–292.
BRETT, R. & BELL, P. M. (1969). *Earth Planet. Sci. Lett.* **6**, 479–482.
BRIDGMAN, P. W. (1927). *Proc. Am. Acad. Arts Sci.* **62**, 207–226.
BROWN, G. E., SUENO, S. & PREWITT, C. T. (1973). *Am. Mineral.* **58**, 698–704.
BUERGER, M. J. (1936). *Z. Kristallogr.* **95**, 83–113.
BURNHAM, C. W. (1966). *Am. Mineral.* **51**, 159–167.
CROMER, D. T. & WABER, J. T. (1974). In *International Tables for X-ray Crystallography*, Vol. IV, pp. 71–147. Birmingham: Kynoch Press.
DOLLASE, W. A. (1965). *Z. Kristallogr.* **121**, 369–377.
EVANS, H. T. JR (1970). *Science*, **167**, 621–623.
FINGER, L. W., HADIDIACOS, C. G. & OHASHI, Y. (1973). *Carnegie Inst. Washington Yearb.* **72**, 694–699.
FINGER, L. W. & KING, H. (1978). *Am. Mineral.* **63**, 337–342.
FINGER, L. W. & PRINCE, E. (1975). *Natl Bur. Stand. (US) Tech. Note* 854.
GOODENOUGH, J. B. (1963). *Magnetism and the Chemical Bond.* New York: Interscience.
GOSSELIN, J. R., TOWNSEND, M. G. & TREMBLAY, R. J. (1976). *Solid State Commun.* **19**, 799–803.
GOSSELIN, J. R., TOWNSEND, M. G., TREMBLAY, R. J. & WEBSTER, A. H. (1976). *J. Solid State Chem.* **17**, 43–48.
GRØNVOLD, F. & HARALDSEN, H. (1952). *Acta Chem. Scand.* **6**, 1452–1469.
HAMILTON, W. C. (1959). *Acta Cryst.* **12**, 609–610.
HARALDSEN, H. (1941). *Z. Anorg. Allg. Chem.* **246**, 195–226.
HORWOOD, J. L., TOWNSEND, M. G. & WEBSTER, A. H. (1976). *J. Solid State Chem.* **17**, 35–42.
HUBBELL, J. H., MCMASTER, W. H., KERR DEL GRANDE, N. & MALLETT, J. H. (1974). *International Tables for X-ray Crystallography*, Vol. IV, pp. 47–70. Birmingham: Kynoch Press.
JELLINEK, F. (1959). *Österr. Chem. Ztg.* **60**, 311–321.
KADIJK, F. & JELLINEK, F. (1969) *J. Less-Common Met.* **19**, 421–430.
KING, D. A. & AHRENS, T. J. (1973). *Nature (London) Phys. Sci.* **243**, 82–84.

KING, H. E. JR (1979). PhD Thesis, State Univ. of New York at Stony Brook.
KING, H. E. JR & FINGER, L. W. (1979). *J. Appl. Cryst.* **12**, 374–378.
KING, H. E. JR & PREWITT, C. T. (1980). *Rev. Sci. Instrum.* **51**, 1037–1039.
KING, H. E. JR, VIRGO, D. & MAO, H. K. (1978). *Carnegie Inst. Washington Yearb.* **77**, 830–835.
KULLERUD, G., BELL, P. M. & ENGLAND, J. L. (1965). *Carnegie Inst. Washington Yearb.* **64**, 197–199.
MERRILL, L. & BASSETT, W. A. (1974). *Rev. Sci. Instrum.* **45**, 290–294.
NAVROTSKY, A. (1980). *Geophys. Res. Lett.* **7**, 709–711.
PICHULO, R. O. (1978). PhD Thesis, Columbia Univ.
PICHULO, R. O., WEAVER, J. S. & TAKAHASHI, T. (1976). *Meteoritics*, **11**, 351 (abstract).
PIERMARINI, G. J., BLOCK, S. & BARNETT, J. D. (1973). *J. Appl. Phys.* **44**, 5377–5382.
PIERMARINI, G. J., BLOCK, S., BARNETT, J. D. & FORMAN, R. A. (1975). *J. Appl. Phys.* **46**, 2774–2780.
PRINCE, E. & NICHOLSON, W. L. (1978). *Am. Crystallogr. Assoc. Program and Abstracts*, **6**, 37 (abstract).
PUTNIS, A. (1974). *Science*, 439–440.
RAJAMANI, V. & PREWITT, C. T. (1974). *Can. Mineral.* **2**, 253–257.
ROBIE, R. A. & WALDBAUM, D. R. (1968). *Geol. Surv. Bull.* 1259. Washington: US Printing Office.
ROBINSON, K., GIBBS, G. V. & RIBBE, P. H. (1971). *Science*, **172**, 567–570.
SELTE, K. & KJEKSHUS, A. (1973*a*). *Acta Chem. Scand.* **27**, 1448–1449.
SELTE, K. & KJEKSHUS, A. (1973*b*). *Acta Chem. Scand.* **27**, 3195–3206.
SHAW, G. H. (1978). *J. Geophys. Res.* **83**, 3519–3523.
SPARKS, J., MEAD, W. & KOMOTO, T. (1962). *J. Phys. Soc. Jpn*, **17** (Suppl. B1), 249–252.
TAYLOR, L. A. (1970). *Carnegie Inst. Washington Yearb.* **68**, 259–270.
TAYLOR, L. A. & MAO, H. K. (1970). *Science*, 170, 850–851.
TICHÝ, K. (1970). *Acta Cryst.* A**26**, 295–296.
USSELMAN, T. M. (1975). *Am. J. Sci.* **275**, 278–290.
VISSER, J. W. (1969). *J. Appl. Cryst.* **3**, 89–95.
VORONOV, F. F., VERESHCHAGIN, L. F. & GONCHAROVA, V. A. (1960). *Sov. Phys. Dokl.* **135**, 1280–1283.
WILSON, R. H. & KASPER, J. S. (1964). *Acta Cryst.* **17**, 95–101.
WOLFE, P. M. DE (1957). *Acta Cryst.* **10**, 590–599.
YUND, R. A. & HALL, H. T. (1968). *Mater. Res. Bull.* **3**, 779–784.
YUND, R. A. & HALL, H. T. (1969). *Econ. Geol.* **64**, 420–423.

Acta Cryst. (1982). B**38**, 1887–1890

Structure du Tétrathiophosphate de Lithium

PAR RENÉ MERCIER, JEAN-PIERRE MALUGANI, BERNARD FAHYS ET GUY ROBERT

Laboratoire d'Electrochimie des Solides, ERA 810, *Université de Franche-Comté*, 25030 *Besançon CEDEX, France*

ET JACQUES DOUGLADE

Laboratoire de Chimie Physique, Université de Franche-Comté, 25030 *Besançon CEDEX, France*

(*Reçu le* 12 *octobre* 1981, *accepté le* 5 *février* 1982)

Abstract

Li_3PS_4 crystallizes in the orthorhombic system, space group *Pnma*, with $a = 13{\cdot}066$ (3), $b = 8{\cdot}015$ (2), $c = 6{\cdot}101$ (2) Å, $V = 639$ Å^3, $Z = 4$, $d_m = 1{\cdot}85$, $d_x = 1{\cdot}87$ Mg m^{-3}. With Mo $K\bar{\alpha}$ radiation ($\lambda = 0{\cdot}71069$ Å, $\mu = 1{\cdot}5$ mm^{-1}), the structure was refined to $R = 0{\cdot}046$ with 255 independent reflexions ($\theta < 30°$). Tetrahedral PS_4^{3-} anions (mean P–S length 2·050 Å) are centered on mirror planes; three kinds of Li^+ ions are revealed in the asymmetric unit: Li(1) in a fully filled site (tetrahedral coordination: Li···S $\simeq$ 2·46 Å); and Li(2) and Li(3) with occupancy factors of 0·7 and 0·3 respectively, so that diffusion of Li^+ through Li(2)–Li(3)–Li(2) tunnels with a 2·52 Å jump between vicinal sites could be expected.

Introduction

Le système $(Li_2S)_x$–$(P_2S_5)_{1-x}$ permet d'obtenir des verres dans un domaine de concentrations ($0{,}60 < x < 0{,}72$) qui présentent une conductivité ionique par les ions Li^+ particulièrement remarquable (Mercier, Malugani, Fahys & Robert, 1981). Ainsi les verres de formulation $Li_4P_2S_7$ ($x = 0{,}667$) possèdent-t-ils une

0567-7408/82/071887-04$01.00